

Regular Article - Living Systems

MFG-E8: a model of multiple binding modes associated with ps-binding proteins

Tiffany Suwatthee¹, Daniel Kerr^{1,2,3}, Sofiya Maltseva¹, Charles L. Dulberger⁴, Luke Hyeondo Hwang¹, Benjamin R. Slaw¹, Wei Bu⁵, Binhua Lin^{3,5}, Erin J. Adams^{2,4}, and Ka Yee C. Lee^{1,2,3,a}

- ¹ Department of Chemistry, The University of Chicago, Chicago, IL, USA
- ² Program in Biophysical Sciences, Institute for Biophysical Dynamics, The University of Chicago, Chicago, IL, USA
- James Franck Institute, The University of Chicago, Chicago, IL, USA
- ⁴ Department of Biochemistry and Molecular Biology, The University of Chicago, Chicago, IL, USA
- ⁵ NSF's ChemMatCARS, The University of Chicago, Chicago, IL, USA

Received 12 June 2023 / Accepted 18 October 2023 \odot The Author(s), under exclusive licence to EDP Sciences, SIF and Springer-Verlag GmbH Germany, part of Springer Nature 2023

Abstract Membrane-binding proteins often associate with lipid membranes through a singular binding interface which is generally modeled as a two-state system: bound or unbound. However, even a single interface can engage with more than one mode of binding since a variety of interactions can contribute to the binding event. Unfortunately, the ability to clearly delineate the different binding modes of a singular binding interface has been elusive with existing models. Here, we present a study on milk fat globule EGF factor 8 (MFG-E8), which belongs to a class of proteins that identifies and binds phosphatidylserine (PS). These proteins detect membrane dysregulation implicated in exposed PS in apoptosis and malignant cells. In order to elucidate the factors affecting the binding of MFG-E8, we used a model system consisting of a series of lipid vesicles with varying PS mole fraction to identify the sensitivity of MFG-E8's binding affinity to changes in electrostatics using a tryptophan fluorescence spectral shift assay. Using a newly developed model, we experimentally identified three binding modes, each associated with a different number of PS lipids, with its cooperativity for binding being enhanced by the availability of negatively charged lipids. X-ray reflectivity experiments additionally suggest that MFG-E8's binding modes are influenced by membrane packing. The protocols established for elucidating MFG-E8's interaction with lipid membranes under different membrane conditions can be applied to the study of other membrane-binding proteins that target specific membrane attributes, such as fluidity and electrostatics, and help elucidate these membrane targeting mechanisms and their subsequent binding events.

1 Introduction

Membrane-binding proteins are responsible for signal transduction as well as protein and membrane trafficking through electrostatic and hydrophobic interactions, specific lipid headgroup binding, and shape complimentary binding mechanisms [1]. Most of these proteins have a singular binding interface in which they directly interact with a specific lipid headgroup, such as phosphatidylserine (PS), the most abundantly negatively charged lipid in cell membranes. Healthy cells actively confine PS to the inner leaflet of the cell membrane. However, under apoptosis or other immune responses.

This article is dedicated to Fyl Pincus who has made many important contributions to soft matter and biological physics. His scientific achievements, insights and mentoring have inspired and enriched many, and have made a lasting impact on our community.

Published online: 24 November 2023

PS flips out to the outer leaflet as a signal for proteins to engage with the cell. Immune cells are known to use PS as an engulfment signal in apoptosis, but how the immune system distinguishes between PS exposure in apoptotic vs. activated cells is unknown [2, 3].

PS-binding proteins can undertake several different orientations upon interacting with the membrane. Proteins such as protein kinase C α (PKC α), sphingokinase-1 (SK1), phospholipase A2 (PLA2), transmembrane immunoglobulin and mucin domain (Tim) proteins, and milk fat globule epidermal growth factor-factor 8 (MFG-E8) insert into the membrane upon PS-binding [4–12]. This insertion can occur at varying positions and depths depending on the protein's direct interaction with PS. PKC α can be targeted to the membrane and activated in several different ways: Ca²⁺ coordination, phorbol ester-induction, phosphorylation, and adapter proteins, all of which cause different binding mechanisms to PS in the membrane [7]. SK1 is active in both its dimeric and monomeric forms;



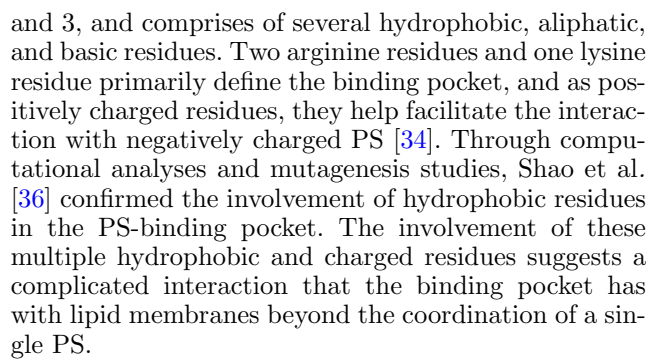
^a e-mail: kayeelee@uchicago.edu (corresponding author)

however, it only coordinates a single PS upon membrane binding so it must have different orientations at the membrane due to its different mechanisms for binding [8, 9]. Geng et al. [10] found that PLA2 positions itself and inserts into the membrane differently depending on the number of PS accessible on the membrane. They reported that an increase in PS availability decreases insertion into the membrane. Previous work in our group has shown that the binding of Tim proteins is dependent on four factors: Ca²⁺ coordination, hydrophobic contacts, bilayer packing, and electrostatic interactions with anionic lipids [11]. Tim 1, Tim 3, and Tim 4 each has minute differences in their binding interactions with the membrane, however, in characterizing the binding interface of Tim 1, molecular dynamic simulations suggest that Tim 1 can bind to the membrane in multiple configurations [12, 13].

Within this class of proteins that identify and bind to PS, we present MFG-E8, also known as lactadherin, as a model of how various factors can contribute to PS-binding and result in a multi-mode binding mechanism to the lipid membrane. MFG-E8 is involved in the clearance of apoptotic cells by targeting the exposed PS of a membrane and connecting it with the integrin of a macrophage, enhancing the engulfment of the apoptotic cell by phagocytes [5, 6, 14–16]. Additionally, MFG-E8 has been found to be involved in several other cellular functions including blood coagulation, cell fusion, inflammation, and the clearance of vesicular debris, such as platelet derived vesicles and the photosensitive outer segments in the mammalian retina [14, 17–20]. MFG-E8 has also been shown to promote obesity by mediating the uptake of dietary fats and serum fatty acids [21]. Its deficiency has been linked to various autoimmune diseases, Alzheimer's disease, Parkinson's disease, neural inflammation, neuron loss, diabetes, and cancer [22-29].

Full-length MFG-E8 contains one to three EGF-like domains at the N-terminus, and two C domains (C1 and C2) on the C-terminus [30]. Depending on the presence of a proline- or a threonine-rich domain, it can have a long and short splice variant [31]. Its EGF-like domains bind to $\alpha v\beta 3$ and $\alpha v\beta 5$ integrins on macrophages, and its C1 and C2 domains bind to exposed PS on apoptotic cells, though MFG-E8 mainly interacts with PS-containing membranes through its C2 domain [32].

The crystal structure of bovine MFG-E8 has been obtained by x-ray [33, 34], and the solution structure of the C2 domain of the murine MFG-E8 was resolved by NMR [34]. These structures provide a basis for molecular interpretations of the C2 domain interaction with lipid membranes. The PS-binding pocket located in the C2 domain of the protein is conserved throughout several different species including human, bovine, and murine [35]. The C2 domain is composed of 164 residues and has a secondary structure of beta sheets that form a beta-barrel-like structure. Ye et al. [34] characterized the interaction of MFG-E8 with lipid micelles composed of short-chained PS and discovered a surface on the C2 domain that directly interfaces with the micelles. This putative PS-binding pocket is located between loops 2



We used a multipronged approach to characterize the binding of the C2 domain to large unilamellar vesicles (LUVs) containing PS. Binding was measured using a tryptophan fluorescence assay based on the intrinsic fluorescence of the binding domain. We investigated the influence of two elements involved in the molecular recognition of apoptotic membranes: PS percentage and membrane packing. By fitting our data using a robust binding model (see supplement), we were able to tease out the different binding modes as well as the conditions under which a certain mode is dominant. We found that the multiple binding modes MFG-E8 has for PScontaining membranes are distinguished by the number of PS specifically coordinated. MFG-E8 also seems to have a different binding orientation at the surface of a loosely packed membrane than one that is more tightly packed, as gleaned from our x-ray reflectivity data. Together these results indicate that MFG-E8 may utilize multiple binding modes dependent on the electrostatic and membrane packing conditions to target specific PS-presenting membranes.

2 Results

2.1 Multiple binding modes of MFG-E8 (1-, 2-, and 3-PS states)

We measured the shift of MFG-E8's tryptophan fluorescence spectra to monitor the association of the protein with membranes composed of mixtures 1-palmitoyl-2-oleoyl-sn-glycero-3-phosphocholine of (POPC). and 1-palmitovl-2-oleovl-sn-glycero-3phosphatidylserine (POPS), varying from 0 to 40 mol % of POPS (subsequently referred to as PS), within a range of 4–1200 μ M of lipid vesicles [L]. We initially determined the bound fraction of protein as a function of [L] from tryptophan fluorescence data analyzed using Eq. 1, which assumes the measured spectra being only composed of a combination of two spectra corresponding to the bound and unbound states of the protein (Fig. S1c).

$$F(\lambda) = b * B(\lambda) + (1 - b) * U(\lambda) \tag{1}$$

where $F(\lambda)$ is the protein spectrum in question, b is the fraction of protein bound, $B(\lambda)$ is the maximally



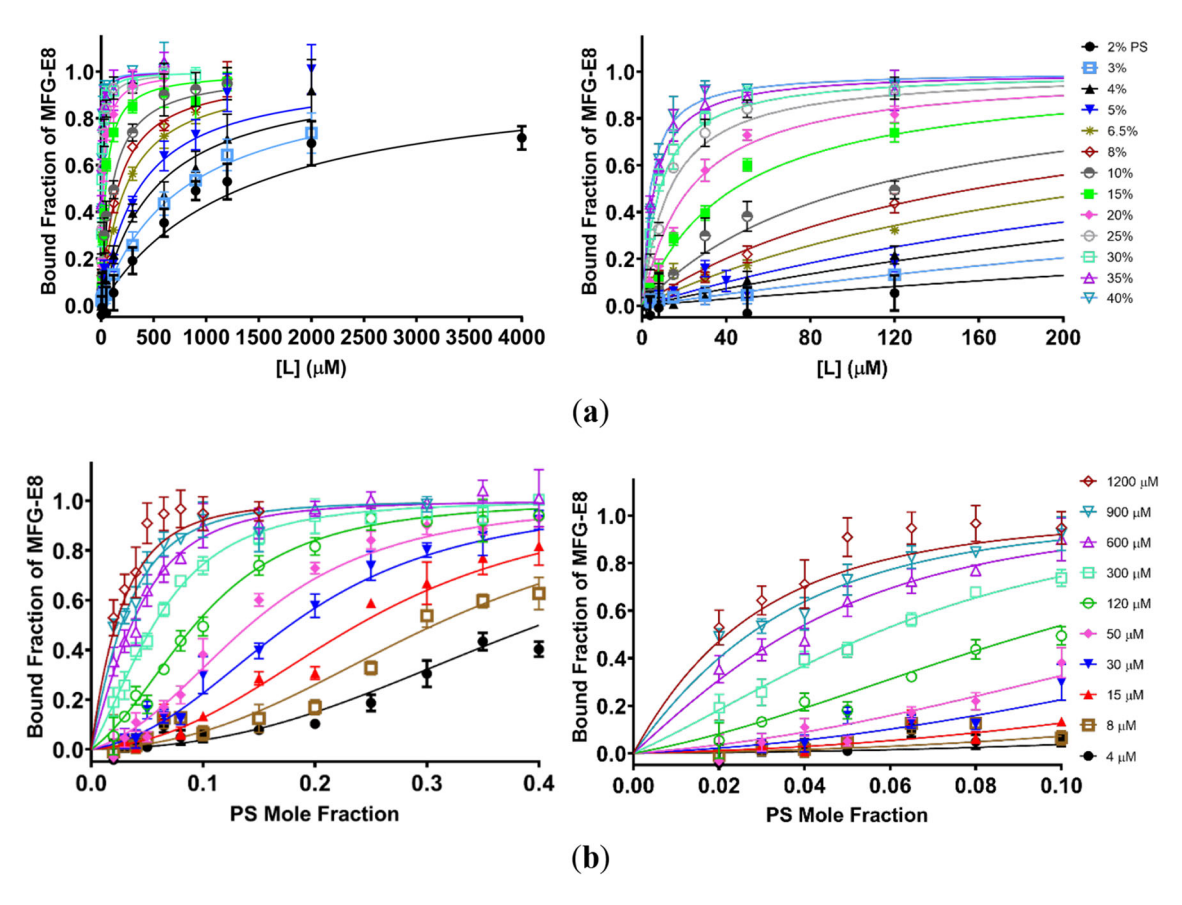


Fig. 1 Binding of MFG-E8 to POPC:POPS vesicles of various PS mole fractions as a function of **a** left: total lipid concentration, right: low lipid concentration (with PS mole fraction in the legend) and **b** left: total PS mole fraction,

right: low PS mole fraction (with total lipid concentration in the legend). Both panels ${\bf a}$ and ${\bf b}$ depict the same underlying data, and error bars represent standard errors of the mean

bound spectrum, and $U(\lambda)$ is the free protein spectrum. However, the maximally bound spectra, obtained by increasing [L] until the spectra cease to change, vary depending on the membrane composition, namely the mole fraction of PS present (Fig. S2). This suggests that the insertion of tryptophan residues of MFG-E8 was dependent on the local lipid environment. We have therefore analyzed our data by applying Eq. 1 to each lipid composition independently, i.e., assuming that each PS mole fraction has a unique bound spectrum independent of [L]. We subsequently fit the data to Eq. 2, which describes the binding dependence on both lipid concentration and lipid composition simultaneously with a shared set of parameters, K_n , and accounts for the varying maximally bound spectra with a normalization parameter for each PS mole fraction, $b_{\max}(\{PS\})$:

$$\frac{b}{b_{\max}(\{PS\})} = \frac{[L] \sum_{n} \frac{\{PS\}^{n}}{K_{n}}}{1 + [L] \sum_{n} \frac{\{PS\}^{n}}{K_{n}}}$$
(2)

where $\{PS\}$ is the mole fraction of PS in the membrane and K_n is the equilibrium constant corresponding to the

bound state associated with n number of PS. For each measured PS mol fraction, we found that the binding of MFG-E8 exhibited non-cooperative binding in the variable [L], as shown in Fig. 1a. This single-site binding dependence on [L] is emergent from Eq. 2 (see supplement) and is expected as the total lipid concentration is a proxy for the vesicle concentration and a single MFG-E8 can only associate with one vesicle at a time because it only has a singular lipid-binding interface incapable of associating with more than one lipid surface.

However, replotting the binding as a function of the PS mole fraction reveals a more complicated dependence on PS, suggesting the presence of more than one PS-binding mode. Upon fitting the binding curves to Eq. 2, we reveal the presence of three different PS-binding modes (Fig. 1b). Each binding mode is distinguished by the exponent for its dependence on PS, reflecting the number of PS lipids each mode requires. The relative populations of these PS-binding modes can be visualized from the fits by plotting each individual binding mode at low (4–30 $\mu M)$, middle (50–300 $\mu M)$, and high (600–1200 $\mu M)$ [L], as seen from left to right in Figure 2. At low [L], the binding curve has a sigmoidal shape, which transforms into a hyperbolic shape at high



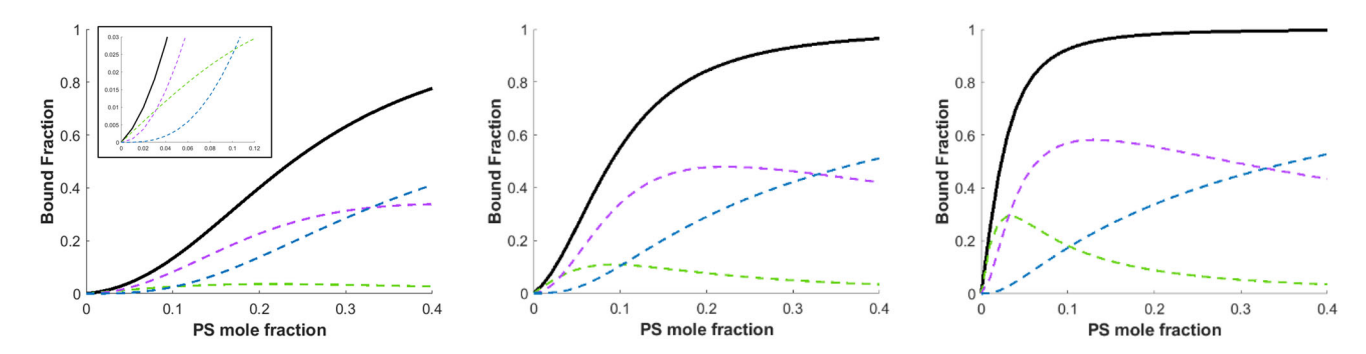


Fig. 2 Visualizations of the PS-binding modes inferred from the fits of the data in Fig. 1. Solid black line represents the overall bound fraction as shown in Fig. 1b, while the green, purple, and blue dashed lines depict the bound

fractions of the 1-PS, 2-PS, and 3-PS modes, respectively. From left to right, plots are shown for [L] = 15 (low), 120 (middle), and 1200 (high) $\mu\rm M$

Table 1 Derived binding parameters for the family of curves for MFG-E8 with various POPS mol% in POPC:POPS vesicles as plotted in Fig. 1 and their 95% confidence intervals

$K_1^{ m eff}$	$40~\mu M~[20,80]$
$K_2^{ m eff}$	$2~\mu\mathrm{M}~[1,19]$
$K_3^{ m eff}$	$0.4~\mu\mathrm{M}~[0.2,0.8]$

[L] (Fig. 2). Separating these binding curves into three inferred fits by decomposing Eq. 2 into three separate equations (Eqs. S6–S8) shows that the 1-PS binding mode is dominant at low {PS}, but quickly transitions to the 2-PS binding mode. At relatively high {PS}, the 3-PS binding mode dominates over all modes. This suggests a positive cooperativity for the 2-PS binding mode, which gives away to the 3-PS binding mode with increasing PS mole fraction.

Despite the appearance of varying sigmoidicity with [L] in the curves of Figure 1b, the cooperativity is solely dependent on {PS}. Figure 2 tracks the relative populations of each binding mode and reveals that the crossover points between each binding mode occurs at the same PS mol% values for all plotted [L] values. This can be seen in Figure 2 at the crossover points between the PS-binding modes occurring at the same {PS} values for all plotted [L] values. The 1-PS binding mode prevails from 0 to 3 mol% PS, the 2-PS mode prevails between 3 and 32.5 mol% PS, and, while the 2-PS mode is dominant, the 1-PS mode prevails over the 3-PS mode between 3 and 10 mol% PS. The appearance of sigmoidicity at a given value of [L] depends on which PS-binding mode is dominant prior to the inflection of the binding curve toward saturation. At high [L], the binding curve starts to deviate from linearity to plateau just as the 2-PS mode becomes dominant, and thus the 1-PS mode's linear dependence on {PS} manifests in the overall bound fraction.

We were able to determine binding constants up to K_3^{eff} , as recorded in Table 1. Each K_i^{eff} corresponds to a different number (i) of PS bound to MFG-E8, which

suggests that MFG-E8 has multiple membrane-bound orientations, depending on the number of PS bound. A closer look at the overall bound fractions (black) in Fig. 2 shows that the initial sigmoidicity in the low PS mole fraction range of both low [L] and middle [L] is due to the dominance of a 2-PS bound state, $K_2^{\rm eff}$ (purple). At high [L], the binding is half-saturated before the 2-PS bound state overtakes the 1-PS bound state, resulting in the overall bound fraction inheriting the linear slope of the 1-PS bound state, $K_1^{\rm eff}$ (green). For the range of [L] that we measured, a 3-PS bound state (blue) dominates at too high of a PS mole fraction to significantly influence the initial sigmoidicity, but it nonetheless affects the rate of saturation, especially at low [L].

2.2 Lipid packing effects

We next investigated the effect of lipid packing on the membrane association of MFG-E8 by probing the structure of the protein-membrane interface. We conducted x-ray reflectivity experiments on MFG-E8-adsorbed lipid monolayers of 1-stearoyl-2-oleoylsn-glycero-3-phosphocholine (SOPC) and 1-stearoyl-2oleoyl-sn-glycero-3-phospho-L-serine (SOPS) deposited at an air-water interface on a Langmuir trough. SOlipids were used in place of PO-lipids because they are similarly mono-unsaturated, but with longer saturated acyl tails that help reduce oxidation and radiation damage done by the x-ray beam [37, 38]. With an adjustable barrier that allowed us to control the total area spanned by the monolayer, we could set and maintain the surface pressure of the monolayer both in the presence and absence of MFG-E8. The output of these experiments is the reflectance of the x-rays over a range of incident angles (expressed as the momentum transfer, Q_z). Because reflectivity measures the elastic scattering normal to an interface, it is therefore sensitive to the change in electron density along the direction normal to the interface.

X-ray reflectivity measurements were taken at surface pressures of 20 and 30 mN/m of 70:30 SOPC:SOPS



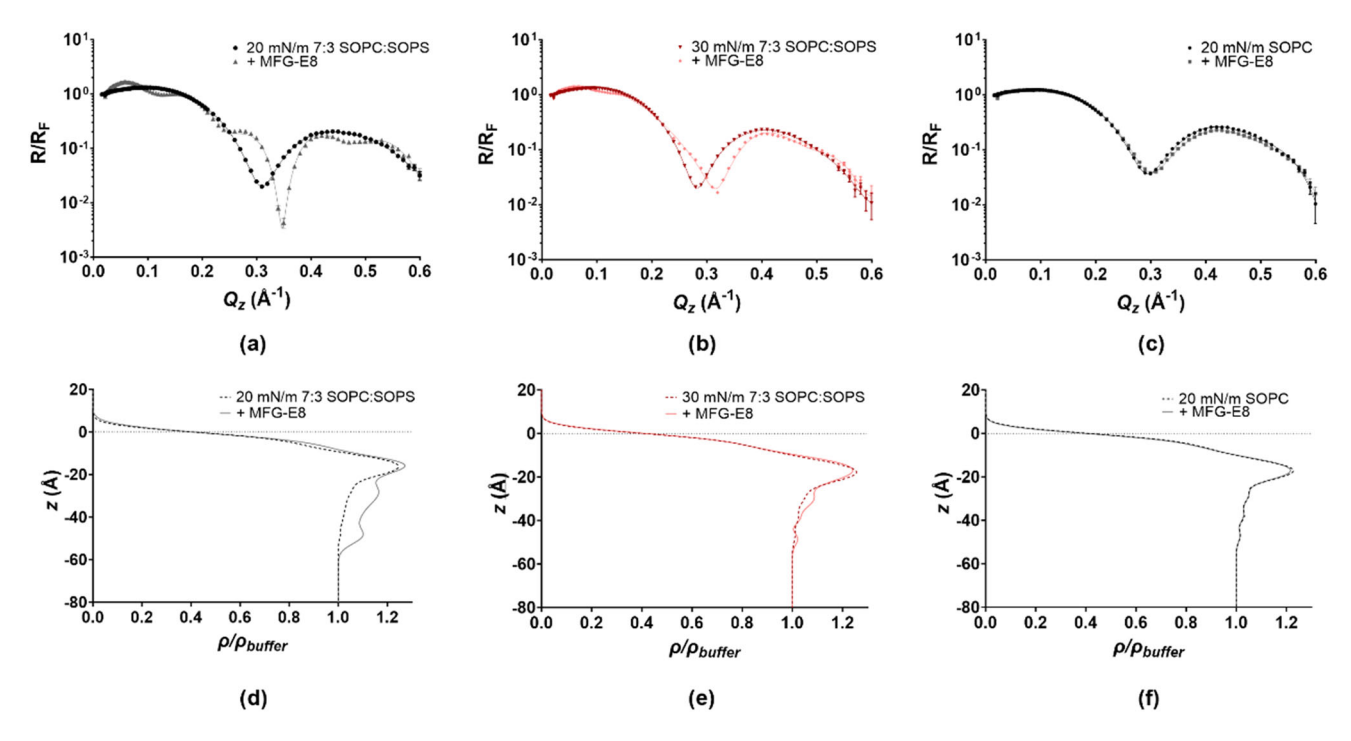


Fig. 3 X-ray reflectivity of MFG-E8 with 7:3 SOPC:SOPS and SOPC monolayers at various surface pressures. Fresnel normalized reflectivity curves obtained from a 7:3 SOPC:SOPS monolayer at surface pressures of **a** 20 mN/m and **b** 30 mN/m with and without 56 nM MFG-E8 in the subphase. **c** Fresnel normalized reflectivity curves obtained

from a SOPC monolayer at a surface pressure of 20 mN/m with and without 56 nM MFG-E8 in the subphase. The corresponding electron density profiles for the 7:3 SOPC:SOPS monolayer panels (a) and (b) at d 20 mN/m and e 30 mN/m. f The corresponding electron density profile for the SOPC monolayer of panel (c)

monolayers with and without MFG-E8 (Fig. 3a and b); embedded in the reflectivity data is the change of the electron density in the direction perpendicular to the interface. The addition of MFG-E8 resulted in significant changes to the reflectivity, namely a shift of the maximum peak to lower Q_z , and the emergence of higher frequency components. None of these changes were induced by MFG-E8 on monolayers composed solely of SOPC (Fig. 3c), which confirms that MFG-E8 does not bind with PC lipid headgroups. These features are consistent with a thickening of the interfacial structure, as a lower value in reciprocal space, Q_z , corresponds to a greater length in real space. The high frequency component in the reflectivity also potentially suggests a highly featured electron density.

In order to obtain a more detailed picture of the interfacial structure, we analyzed the x-ray reflectivity data using the model-independent methodology of StochFit [39]. This analysis provided electron density profiles of the interfacial structure (Fig. 3d–f) most consistent with the reflectivity curves from which they were derived (Fig. 3a–c, respectively). For these electron density profiles, we have defined z=0 to be the top edge of the lipid monolayer-air interface. The electron density profiles for the lipid monolayers without MFG-E8 comprises of two key features, a quick rise in electron density to a shallow plateau at small z, followed by another steep rise that achieves a maximum at ~ 15 Å

beneath the lipid monolayer-tail interface and falls to the electron density of the buffer at ~ 20 Å beneath the lipid monolayer-air interface. These features are consistent with the established two-box model for the electron density of lipid monolayers, and the thickness is consistent with those we have previous measured for this lipid composition [37, 38, 40, 41]. In this two-box model, the shallow plateau corresponds to the tail group region of the lipid monolayer while the subsequent maximum corresponds to the head group region.

The presence of MFG-E8 in the 70:30 SOPC:SOPS monolayer was indicated as a pronounced increase of electron density below the head group region, roughly 30 Å in thickness (Fig. 3d and e). This is consistent with an adsorbed layer of MFG-E8 at the lipid monolayerbuffer interface that slightly buries into the monolayer. The added electron density beneath the head group region contains multiple local maxima and minima and is likely responsible for the observed high frequency component in the reflectivity curves. We also observed an increase of the maximum electron density, corresponding to the head group region of the lipid monolayer. This peak is shifted to lower z for a surface pressure of 30 mN/m but shifted to higher z for a surface pressure of 20 mN/m. From this, we can infer that MFG-E8 inserts more deeply at 20 mN/m than at 30 mN/m. Additionally, the electron density of the protein beneath the head group region is not the same



for these surface pressures, suggesting that the protein has a different interfacial structure as a function of surface pressure. Since the monolayer area is expanded or compressed in order to change the surface pressure, the lipid packing also changes with surface pressure and thus the protein might adopt different orientations on the membrane depending on its ability to insert. It is not possible to conclude whether these electron density profiles correspond to changes in the tertiary structure and orientation of a defined bound state or changes in a distribution over an ensemble of multiple, distinct bound states. In either case, these different interfacial structural features suggest that MFG-E8 has different binding modes that are sensitive to changes in lipid packing.

3 Discussion

Upon determining the true bound fractions of MFG-E8, the data were fit to a binding equation (Eq. 2) that accounted for the dependence on PS mole fraction as well as total lipid concentration. We were able to determine three binding constants for MFG-E8: K_1^{eff} , K_2^{eff} , and K_3^{eff} , corresponding to the 1-PS, 2-PS, and 3-PS bound states, respectively. The dependence of the three binding modes on PS mole fraction manifests as an apparent dependence of the sigmoidicity on the lipid concentration, [L]. At high [L], the binding inflects from linearity to saturation while the 1-PS binding mode is most dominant. At low [L], the binding transitions from the linear dependence of the 1-PS mode to the square and cubic dependence of the 2-PS and 3-PS modes prior to saturation, giving rise to the overall sigmoidal shape of the binding curve. The use of Eq. 2 clarifies that the source of changing sigmoidicity is not due to changing vesicle concentration, [L], but rather an underlying variable cooperativity for PS. Thus, in simultaneously accounting for the dependence on [L] and the PS mole fraction, our model provides a clearer picture of the underlying membrane interactions in MFG-E8 binding evidenced by its ability to delineate multiple binding modes in manners different from standard binding models. Traditional binding models view cooperative binding interactions as a collection of binding sites whose affinities are modified based on the occupation of their neighboring binding sites. However, our model describes a membrane-binding interaction of a singular interface with multiple, distinct binding parameters that in combination manifest as cooperativity.

A "N-PS bound" state does not assume that N-PS molecules are directly interacting with MFG-E8. Given that there exists a singular PS-binding pocket on the C2 domain, the protein only directly interacts with one PS in the binding pocket. However, an increase in the number of PS available to the protein contributes to its binding by creating a cooperative electrostatic effect that aids and stabilizes the direct binding event involving a single PS. Therefore the 2-PS and 3-PS states are "cooperative" binding modes that increase the binding

affinity of MFG-E8 to PS due to the increased electronegative charge on the surface of the membrane.

An additional example to this family of PS-binding proteins is coagulation factor V, which is in the same discoidin-like categorization as MFG-E8. Coagulation factor V is a Ca^{2+} -independent PS-binding protein that has both a procoagulant and anticoagulant function in the blood. The crystal structure of its C2 domain is remarkably similar to the crystal structure of the C2 domain structure of both human lactadherin and bovine lactadherin, and thus is likely very similar to the C2 domain structure of murine MFG-E8 as well. The beta-barrel-like structure of factor V contains two loops that create a binding interface for 1 PS and inserts two tryptophans into the membrane like MFG-E8. Its binding to PS has also been found to be highly cooperative with increasing PS mole fraction. Its crystal structure shows 1 PS in its binding pocket, and therefore, it must also utilize the electrostatic effect afforded by the presence of additional PS molecules to enhance binding [42-44].

Our x-ray reflectivity measurements and analysis suggest that under different lipid packing conditions, the interfacial structure of the bound protein is different. This is indicated by the different peak heights and shapes of each electron density profile of bound protein for 20 and 30 mN/m. This may possibly be due to different orientations of the protein for its multiple binding modes. The fact that the electron density profiles derived from x-ray reflectivity changed even though the electrostatic identity of membrane was the same (70:30 PC:PS) suggests that membrane packing plays an important role in determining the multiple binding modes of MFG-E8.

Like MFG-E8, coagulation factor V, as well as other PS-binding proteins like PKC α , SK1, PLA2, and Tim proteins, must have a more complicated binding interaction than a single lipid-binding event. Protein–lipid binding cannot be described as simply bound and unbound, but rather a combination of molecular mechanisms that must be accounted for when extrapolating the binding modes of these proteins. Thus, for PS-binding proteins, a complex approach that combines two or more contributing binding interactions is necessary to thoroughly understand these interactions.

4 Conclusions

The interactions of MFG-E8 with lipid membranes under different membrane conditions offer insight into the mechanism of MFG-E8's sensitivity to electrostatics and packing properties of lipid membranes and presents an example of how PS-binding proteins can have compounding interactions with lipid membranes. Our results indicate that MFG-E8 has multiple binding modes dependent on the number of PS available at the surface of the membrane and the lipid packing of the membrane. The introduction of multiple binding modes for PS-binding proteins expands the ability



to characterize and quantify the binding of other similar PS-binding proteins like coagulation factor V, PKC α , SK1, PLA2, and Tim proteins. The manifestation of binding modes under different membrane conditions can help elucidate how MFG-E8 differently binds to membranes as it facilitates various physiological processes.

5 Materials and methods

5.1 Lipids and chemicals

Analytical grade 4-(2-hydroxyethyl)-1piperazineethanesulfonic acid (HEPES), NaCl. solvents chloroform. methanol. and including procured acetone were from Fisher Scientific. 1-palmitoyl-2-oleoyl-sn-glycero-3-Lipids including (POPC), 1-palmitoyl-2-oleoyl-snphosphocholine glycero-3-phosphatidylserine (POPS). 1-stearovl-2-oleovl-sn-glycero-3-phosphocholine (SOPC). and 1-stearoyl-2-oleoyl-sn-glycero-3-phospho-L-serine (SOPS) were obtained from Avanti Polar Lipids (Alabaster, AL). Lipid stocks were prepared by dissolving dry lipids in chloroform, then evaporating the solvent under a stream of Argon gas, and further in a vacuum desiccator for at least 1 h at room temperature. Chloroform is then reintroduced to the lipid in order to obtain a molar concentration of 6, 9, or 12 mM lipid. Total lipid concentration was determined by using Molybdenum Blue [48]. The buffer in most studies was 10 mM HEPES (pH 7.4) 150 mM NaCl.

5.2 Preparation of large unilamellar vesicles (LUV)

LUV were produced by extrusion [11]. Lipids in the powder form were dissolved in chloroform, mixed at the desired concentration and composition, then dried to form a thin film inside the glass vials under argon flow. The lipids were further dried under vacuum for at least 1 h at room temperature. Lipid mixtures were then suspended in HBS and vortexed at a moderate speed for 1 h at 37 °C. The lipid/buffer mixtures were then subjected to five freeze—thaw cycles using a dry ice/ethanol slurry. Finally, the lipids were extruded 23 times using 100-nm-diameter filters (Avanti Polar Lipids) on a 50 °C heat block. Vesicle diameter and polydispersity were around 120 nm and 10%, respectively, as determined by dynamic light scattering (Zen3600 Malvern Nano Zetasizer). The total lipid concentration was determined by using Molybdenum Blue [48].

5.3 MFG-E8 C2 domain expression and purification

The cDNA for the *Mus musculus* MFG-E8L C2 domain containing a hexa-histidine tag at the C-terminus in the pET29b vector was a gift from Dr. Sreekanth Rajan and Dr. Yoon Ho Sup at Nanyang Technological University,

Singapore. The plasmid was transformed into *E. coli* BL21 (DE3) cells for recombinant protein expression.

Expression and purification of the MFG-E8L C2 domain was performed essentially as described previously [34]. Briefly, transformants were selected on a LB agar plate containing 30 µg/ml kanamycin and a single colony was inoculated into a 50 mL LB + kanamycin starter culture and grown at 37 °C in a shaker at 220 rpm for 15 h. 20 mL of the starter culture was inoculated into 1 L of LB media containing kanamycin and grown to an $OD_{600} \sim 0.7$. At this point, the culture was transferred to a room temperature (~ 25 °C) shaker and cells were induced to express the MFG-E8L C2 domain via the addition of 1 mM Isopropyl β -D-1thiogalactopyranoside (IPTG). After 4 h of growth, the culture was harvested via centrifugation at 6,000 × g for 10 min in a Beckman JLA-8.1 rotor. After removing the supernatant, cell pellets were frozen at -80 °C.

Cell pellets were resuspended at 4 °C via stirring with 10 mL/g of cell pellet in suspension buffer (20 mM Na-PO₄, pH 7.3, 0.5 M NaCl, 1 mM phenylmethylsulfonyl fluoride (PMSF) and a pinch of DNAse). Cell lysis was performed by passing the resuspension through a microfluidizer (EmulsiFlex-C5 homogenizer, AVESTIN) three times. Cell lysate was centrifuged at 22,000 rpm for 30 min using a Beckman JA-25.50 rotor. The supernatant was brought up to 25 mM imidazole, pH 7 and the MFG-E8L C2 domain was extracted from the supernatant via batch binding for 1 h at 4 °C with 3 mL of Ni-nitrilotriacetic acid (NTA) agarose beads (Qiagen). Ni–NTA beads were then collected and washed with 3 bed volumes of washing buffer (20 mM Na-PO₄, pH 6.5, 0.5 M NaCl, 1 mM PMSF and 25 mM imidazole) and eluted with elution buffer (20 mM Na-PO₄, pH 6.5, 0.5 M NaCl and 0.2 M imidazole). Fractions containing the eluted protein was then pooled and desalted into 20 mM Na-PO₄, pH 6.5, 0.5 M NaCl via Econo-Pac 10DG desalting prepacked gravity flow columns (Bio-Rad) to remove the imidazole and concentrated via centrifugal filter units (Millipore) to 1 mL for two 0.5 mL injections onto a S75 size exclusion column. The MFG-E8L C2 domain elutes off the S75 column at ~ 22 mL, which is much later than would be predicted based on the size of the MFG-E8L C2 domain. Protein fractions were then analyzed by 12% sodium dodecyl sulfate-polyacrylamide gel electrophoresis (SDS-PAGE) and the protein concentration was calculated via the Bradford protein assay (Bio-Rad), or the hypothetical extinction coefficient generated by the ExPASy ProtParam tool. Typical protein yields were ~ 2 mg/L culture medium. The MFG-E8L C2 domain is sensitive to concentration via centrifugal filter units, so protein for experiments was used at the concentration in which it came off the S75 column (\sim $18 \mu M \text{ or } 0.35 \text{ mg/mL}$).

5.4 Tryptophan fluorescence assay

A Horiba Fluorolog-3 spectrophotometer with USHIO Xenon short arc lamp and a 1-cm path-length quartz



cuvette was used with excitation at 280 nm and emission collected from 300 to 420 nm. The sample contained a range of concentrations of total phospholipid (0-1200 µM) and 80 nM protein in 10 mM HBS (pH 7.4) 150 mM NaCl. Experiments were performed at 23 °C. MFG-E8 association with membranes composed of mixtures of mono-unsaturated lipids (POPC and POPS) with PS content varying from 0 to 40 mol %. was monitored by the blue shift of \sim 5 nm and the increase of the quantum yield of its membrane embedded tryptophan residues W26 and W33. Spectrum of lipid and buffer with stirring was first collected. Then spectrum of lipid, buffer, and protein was collected after one minute of equilibration with stirring. Results were only accepted if the lamp current was stable within 10^{-3} microamps for more than 10 min. Experiments were repeated at least 3 times unless denoted otherwise.

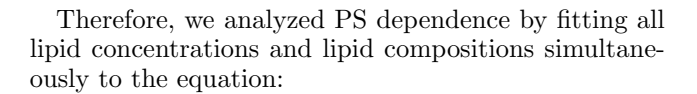
5.5 Fluorescence binding analysis

In order to determine the relative binding affinity of MFG-E8, these tryptophan fluorescence curves are integrated into a plot of tryptophan saturation through a linear combination of the relative intensity of each PS percentage point and the maximum intensity of a given condition. The fraction of tryptophan inserted can be used to extrapolate how much MFG-E8 is bound to the membrane [45].

Two tryptophan side chains (W26 and W33) interact with the lipid membrane upon binding [34], at which point the tryptophan residues insert into the lipid tail group region. As they enter a less polarizable environment, the tryptophan residues fluoresce at a higher intensity and a lower wavelength [46]. If we assume that there are only two tryptophan emitting states, corresponding to the bound and unbound protein, the fraction of protein with buried tryptophan b, can be calculated using the following expression:

$$F(\lambda) = b * B(\lambda) + (1 - b) * U(\lambda) \tag{1}$$

where $F(\lambda)$ is the protein spectrum in question, $B(\lambda)$ is the maximally bound spectrum, and $U(\lambda)$ is the free protein spectrum. This expression is only valid if the average bound spectrum does not vary with changing experimental conditions. However, we found that this was not the case when analyzing tryptophan spectra as a function of varied PS in our system. Therefore, this equation was only used to fit the bound fractions of experiments conducted on the same lipid compositions, i.e., fixed PS mole fraction. In practice, (λ) was approximated using the spectrum corresponding to the condition with the highest tryptophan shift. The bound fraction obtained from this fit is relative to the highest observed binding and is not necessarily the true bound fraction of protein.



$$\frac{b}{b_{\max}(\{PS\})} = \frac{[L] \sum_{n} \frac{\{PS\}^{n}}{K_{n}}}{1 + [L] \sum_{n} \frac{\{PS\}^{n}}{K_{n}}}$$
(2)

where $\{PS\}$ is the mole fraction of PS in the membrane and K_n is the equilibrium constant corresponding to the bound state associated with n number of PS. Here, $b_{max}(\{PS\})$ is the signal corresponding to maximum binding for a given PS mole fraction. b_{max} is treated as a free parameter for each lipid composition while the K_n parameters are constrained to be shared between all lipid compositions.

5.6 X-ray reflectivity experiments

X-ray reflectivity (XR) at the air/liquid interface gives us an electron density profile along the out-of-plane direction of a lipid monolayer in complex with the protein that afford the determination of the different orientations as well as depths of insertion of the protein into the lipid layer. XR experiments were performed at ChemMatCARS of Sector 15-ID at the Advanced Photon Source of Argonne National Laboratory. A custom trough with a movable barrier and surface pressure control loop was used to control the surface pressure of the lipid monolayer. Surface pressure was controlled at two values, 20 and 30 mN/m. A reflectivity scan on the lipid-only system was performed for each film prior to injecting the protein to the subphase. A final concentration of about 56 nM MFG-E8 was injected into the 70 mL subphase. After one hour of equilibration, stirring was stopped and x-ray reflectivity scans were taken within a Q_z (scattering wave vector in the z-direction) range of $0.018-0.55 \text{ Å}^{-1}$ or $0.016-0.65 \text{ Å}^{-1}$. X-ray data were analyzed via StochFit [39] using 40 boxes for a total length of 40 angstroms. All fits converged within 100,000 iterations.

Supplementary Information The online version contains supplementary material available at https://doi.org/10.1140/epje/s10189-023-00372-w..

Acknowledgments We thank Elena Solomaha and Zhiliang Gong for their input into this study. The cDNA for the Mus musculus MFG-E8L C2 domain containing a hexahistidine tag at the C-terminus in the pET29b vector was a gift from Dr. Sreekanth Rajan and Dr. Yoon Ho Sup at Nanyang Technological University, Singapore. C.L.D. and E.J.A. provided lab space, materials, and guidance for protein purification. This work was supported by the National Science Foundation through MCB-1950525 (to K.Y.C.L.) K.Y.C.L. acknowledges support from The University of Chicago Materials Research Science and Engineering Center (NSF/DMR- 2011854) and The University of Chicago Biophysics Core Facility. National Science Foundation's ChemMatCARS Sector 15-ID is principally supported by the National Science Foundation under Grant NSF/CHE-



1834750. Additional National Institutes of Health support was provided under grant No. R01 AI155984 (to E.J.A.). T.S. is grateful for the support of The University of Chicago Chemistry and Biological Chemistry Undergraduate Summer Research Grant (2017–2018) and the Jeff Metcalf Fellowship (2019). S.M. acknowledges support from the National Institutes of Health through the CBI training grant No. 5T32GM008720-20. Use of the Advanced Photon Source was supported by the DOE Office of Science, Office of Basic Energy Sciences, under Contract DE-AC02-06CH11357.

Author contributions

TS, DK, and KYCL designed research. TS, DK, SM, CLD, LHH, and BRS performed research. WB and BL contributed new reagents/analytic tools for x-ray reflectivity at NSF's ChemMatCARS Sector 15-ID. TS and DK analyzed data. TS, DK, and KYCL wrote the paper.

Data availability The datasets generated during the current study are available from the corresponding author on reasonable request.

Declarations

Conflict of interest The authors declare no conflict of interest.

References

- J.H. Hurley, Membrane binding domains. Biochimica et Biophysica Acta (BBA)-Mol. Cell Biol. Lipids 1761(8), 805–811 (2006)
- 2. B. Frey, U.S. Gaipl, The immune functions of phosphatidylserine in membranes of dying cells and microvesicles, in *Seminars in Immunopatholog*. (Springer, Verlag, 2011), pp.497–516
- 3. E.M. Bevers, P.L. Williamson, Getting to the outer leaflet: physiology of phosphatidylserine exposure at the plasma membrane. Physiol. Rev. **96**(2), 605–645 (2016)
- M.A. Lemmon, Membrane recognition by phospholipidbinding domains. Nature 9, 99–111 (2008)
- R. Hanayama et al., Identification of a factor that links apoptotic cells tophagocytes. Nature 417(6885), 182–187 (2002)
- G.G. Borisenko et al., Milk fat globule epidermal growth factor 8 (MFG-E8) binds to oxidized phosphatidylserine: implications for macrophage clearance of apoptotic cells. Cell Death Differ. 11(8), 943–945 (2004)
- 7. M. Medkova, W. Cho, Interplay of C1 and C2 domains of protein kinase $C-\alpha$ in its membrane binding and activation. J. Biol. Chem. **274**(28), 19852–19861 (1999)
- 8. M.J. Pulkoski-Gross, M.L. Jenkins, J.P. Truman, M.F. Salama, C.J. Clarke, J.E. Burke, L.M. Obeid, An intrinsic lipid-binding interface controls sphingosine kinase 1 function [S]. J. Lipid Res. **59**(3), 462–474 (2018)

- R.V. Stahelin, J.H. Hwang, J.H. Kim, Z.Y. Park, K.R. Johnson, L.M. Obeid, W. Cho, The mechanism of membrane targeting of human sphingosine kinase 1. J. Biol. Chem. 280(52), 43030–43038 (2005)
- F. Geng, G. Zhang, Y. Wang, J. Lü, Membrane phosphatidylserine allosterically regulates the cytosolic phospholipase A2 activity via an electrostatic-switch mechanism. Soft Matter 18(11), 2203–2210 (2022)
- D. Kerr, Z. Gong, T. Suwatthee, A. Luoma, S. Roy, R. Scarpaci, H.L. Hwang, M.J. Henderson, K.D. Cao, W. Bu, B. Lin, G.T. Tietjen, T.L. Steck, E.J. Adams, K.Y.C. Lee, How Tim proteins differentially exploit membrane features to attain robust target sensitivity. Biophys. J. J. 120(21), 4891–4902 (2021)
- G.T. Tietjen, J.L. Baylon, D. Kerr, Z. Gong, J.M. Henderson, C.T. Heffern, M. Meron, B. Lin, M.L. Schlossman, E.J. Adams, E. Tajkhorshid, K.Y.C. Lee, Coupling X-ray reflectivity and in silico binding to yield dynamics of membrane recognition by Tim1. Biophys. J.. J. 113(7), 1505–1519 (2017)
- D. Kerr et al., Sensitivity of peripheral membrane proteins to the membrane context: A case study of phosphatidylserine and the TIM proteins. Biochimica et Biophysica Acta (BBA)-Biomembranes. 1860(10), 2126–2133 (2018)
- K. Oshima et al., MFG-E8: origin, structure, expression, functions and regulation, in MFG-E8 and Inflammation. ed. by P. Wang (Springer, Dordrecht, 2014)
- K. Miyasaka, R. Hanayama, M. Tanaka, S. Nagata, Expression of milk fat globule epidermal growth factor 8 in immature dendritic cells for engulfment of apoptotic cells. Eur. J. Immunol.Immunol. 34(5), 1414–1422 (2004)
- A.D. Fuller, L.J. Van Eldik, MFG-E8 regulates microglial phagocytosis of apoptotic neurons. J. Neuroimmune Pharmacol.Neuroimmune Pharmacol. 3(4), 246–256 (2008)
- 17. L.W. Hansen et al., Treatment with milk fat globule epidermal growth factor- factor 8 (MFG-E8) reduces inflammation and lung injury in neonatal sepsis. Surgery 162(2), 349–357 (2017)
- S. Arienti et al., Regulation of apoptotic cell clearance during resolution of inflammation. Front. Pharmacol. Pharmacol. 10, 891 (2019)
- 19. S.K. Dasgupta et al., Lactadherin and clearance of platelet-derived microvesicles. Blood, J. Am. Soc. Hematol. **113**(6), 1332–1339 (2009)
- E.F. Nandrot et al., Essential role for MFG-E8 as ligand for ανβ5 integrin in diurnal retinal phagocytosis. Proc. Nat. Acad. Sci. 104(29), 12005–12010 (2007)
- A. Khalifeh-Soltani et al., Mfge8 promotes obesity by mediating the uptake of dietary fats and serum fatty acids. Nat. Med. 20(2), 175–183 (2014)
- J. Boddaert et al., Evidence of a role for lactadherin in alzheimer's disease. Am. J. Pathol. Pathol. 170(3), 921–929 (2007)
- K. Kinugawa et al., MFGE8 does not orchestrate clearance of apoptotic neurons in a mouse model of Parkinson's disease. Neurobiol. Dis.. Dis. 51, 192–201 (2013)
- M. Fricker et al., MFG-E8 mediates primary phagocytosis of viable neurons during neuroinflammation. J. Neurosci. Neurosci. 32(8), 2657–2666 (2012)



- U. Neniskyte, G.C. Brown, Lactadherin/MFG-E8 is essential for microglia-mediated neuronal loss and phagoptosis induced by amyloid β. J. Neurochem.Neurochem. 126(3), 312–317 (2013)
- 26. A. Das et al., Correction of MFG-E8 resolves inflammation and promotes cutaneous wound healing in diabetes. J. Immunol.Immunol **196**(12), 5089–5100 (2016)
- 27. G. Sugano et al., Milk fat globule—epidermal growth factor—factor VIII (MFGE8)/lactadherin promotes bladder tumor development. Oncogene **30**(6), 642–653 (2011)
- 28. M. Neutzner et al., MFG-E8/lactadherin promotes tumor growth in an angiogenesis-dependent transgenic mouse model of multistage carcinogenesis. Cancer Res. **67**(14), 6777–6785 (2007)
- P. Wang, MFG-E8 and Inflammation (Springer Science & Business Media, Berlin, 2014)
- T. Watanabe et al., Production of the long and short forms of MFG-E8 by epidermal keratinocytes. Cell Tissue Res. 321(2), 185–193 (2005)
- 31. M.H. Andersen, H. Graversen, S.N. Fedosov, T.E. Petersen, J.T. Rasmussen, Functional analyses of two cellular binding domains of bovine lactadherin. Biochemistry **39**(20), 6200–6206 (2000)
- M.H. Andersen et al., Bovine PAS-6/7 binds ανβ5 integrin and anionic phospholipids through two domains. Biochemistry 36(18), 5441–5446 (1997)
- 33. L. Lin, Q. Huai, M. Huang, B. Furie, B.C. Furie, Crystal structure of the bovine lactadherin C2 domain, a membrane binding motif, shows similarity to the C2 domains of factor V and factor VIII. J. Mol. Biol. 371(3), 717–724 (2007)
- 34. H. Ye, B. Li, V. Subramanian, B.-H. Choi, Y. Liang, A. Harikishore, G. Chakraborty, K. Baek, H.S. Yoon, NMR solution structure of C2 domain of MFG-E8 and insights into its molecular recognition with phosphatidylserine. Biochim. Biophys. Acta. Biophys. Acta 1828, 1083–1093 (2013)
- R.P. Nanga, S. Vivekanandan, H.S. Yoon, Expression, purification, and characterization of C2 domain of milk fat globule-EGF-factor 8-L. Protein Expr. Purif. Purif. 52, 329–333 (2007)
- C. Shao et al., Crystal structure of lactadherin C2 domain at 1.7 Å resolution with mutational and computational analyses of its membrane-binding motif. J. Biol. Chem. 283(11), 7230–7241 (2008)
- C.H. Chen, S Málková, S.V. Pingali, F. Long, S. Garde, W. Cho, M.L. Schlossman, Configuration of PKCα-C2 domain bound to mixed SOPC/SOPS lipid monolayers. Biophys. J.. J. 97(10), 2794–2802 (2009)

- Š Málková, F. Long, R. Stahelin, S. Pingali, D. Murray, W. Cho, M. Schlossman, X-Ray reflectivity studies of cPLA2α-C2 domains adsorbed onto langmuir monolayers of SOPC. Biophys. J. J. 89, 1861–1873 (2005)
- S.M. Danauskas et al., Stochastic fitting of specular Xray reflectivity data using StochFit. J. Appl. Crystallogr.Appl Crystallogr 41(6), 1187–1193 (2008)
- Z. Gong, D. Kerr, H.L. Hwang, J.M. Henderson, T. Suwatthee, B.R. Slaw, K.D. Cao, B. Lin, W. Bu, K.Y.C. Lee, Quantitative analysis of total reflection X-ray fluorescence from finely layered structures using XeRay. Rev. Sci. Instrum.Instrum. 88(3), 033112 (2017)
- G. Tietjen, Z. Gong, C.H. Chen, E. Vargas, J.E. Crooks, K.D. Cao, C.T. Heffern, J.M. Henderson, M. Meron, B. Lin, B. Roux, M.L. Schlossman, T.L. Steck, K.Y. Lee, E.J. Adams, Molecular mechanism for differential recognition of membrane phosphatidylserine by the immune regulatory receptor Tim4. Proc. Natl. Acad. Sci. 111, E1463–E1472 (2014)
- S. Macedo-Ribeiro, W. Bode, R. Huber, M.A. Quinn-Allen, S.W. Kim, T.L. Ortel, P. Fuentes-Prior, Crystal structures of the membrane-binding C2 domain of human coagulation factor V. Nature 402(6760), 434–439 (1999)
- 43. W. Lam, and L. Moosavi, Physiology, factor V. (2019)
- W. Cho, R.V. Stahelin, Membrane binding and subcellular targeting of C2 domains. Biochimica et Biophysica Acta (BBA)-Mol. Cell Biol. Lipids 1761(8), 838–849 (2006)
- S. Vanni, L. Vamparys, R. Gautier, G. Drin, C. Etchebest, P.F. Fuchs, B. Antonny, Amphipathic lipid packing sensor motifs: probing bilayer defects with hydrophobic residues. Biophys. J.. J. 104, 575–584 (2013)
- C. Kraft, J. Garrido, L. Leiva-Vega, G. Romero, Quantitative analysis of protein-lipid interactions using tryptophan fluorescence. Sci. Signal. 2, 14 (2009)
- 47. L. Ruggiero et al., Diurnal, localized exposure of phosphatidylserine by rod outer segment tips in wild-type but not Itgb5-/- or Mfge8-/- mouse retina. Proc. Nat. Acad. Sci. 109(21), 8145-8148 (2012)
- 48. W.R. Morrison, A fast, simple and reliable method for the microdetermination of phosphorus in biological materials. Anal. Biochem. 7, 218–224 (1964)

Springer Nature or its licensor (e.g. a society or other partner) holds exclusive rights to this article under a publishing agreement with the author(s) or other rightsholder(s); author self-archiving of the accepted manuscript version of this article is solely governed by the terms of such publishing agreement and applicable law.

